

## Accepted Manuscript

Numerical analysis of effective elastic properties of geomaterials containing voids using 3D random fields and finite elements

Jumpol Paiboon, D.V. Griffiths, Jinsong Huang, Gordon A. Fenton

PII: S0020-7683(13)00244-8

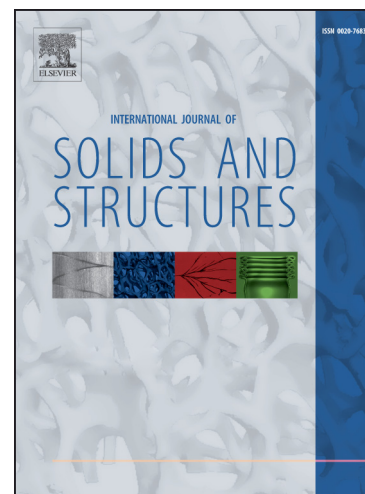
DOI: <http://dx.doi.org/10.1016/j.ijsolstr.2013.05.031>

Reference: SAS 8026

To appear in: *International Journal of Solids and Structures*

Received Date: 1 February 2013

Revised Date: 21 May 2013



Please cite this article as: Paiboon, J., Griffiths, D.V., Huang, J., Fenton, G.A., Numerical analysis of effective elastic properties of geomaterials containing voids using 3D random fields and finite elements, *International Journal of Solids and Structures* (2013), doi: <http://dx.doi.org/10.1016/j.ijsolstr.2013.05.031>

This is a PDF file of an unedited manuscript that has been accepted for publication. As a service to our customers we are providing this early version of the manuscript. The manuscript will undergo copyediting, typesetting, and review of the resulting proof before it is published in its final form. Please note that during the production process errors may be discovered which could affect the content, and all legal disclaimers that apply to the journal pertain.

**Numerical analysis of effective elastic properties of geomaterials  
containing voids using 3D random fields and finite elements**

Jumpol Paiboon<sup>1</sup>, D.V. Griffiths<sup>1,2</sup>, Jinsong Huang<sup>2</sup> and Gordon A. Fenton<sup>3</sup>

1 Department of Civil and Environmental Engineering, Colorado School of Mines,  
Golden, CO, 80401 USA

2 Australian Research Council Centre of Excellence for Geotechnical Science and Engineering,  
University of Newcastle, Callaghan NSW 2308, Australia

3 Department of Engineering Mathematics, Dalhousie University, Nova Scotia B3J 2X4, Canada

**Abstract**

The purpose of the study is to investigate the influence of porosity and void size on effective elastic geotechnical engineering properties with a 3D model of random fields and finite element. The random field theory is used to generate models of geomaterials containing spatially random voids with controlled porosity and void size. A “tied freedom” analysis is developed to evaluate the effective Young’s modulus and Poisson’s ratio in an ideal block material of finite elements. To deliver a mean and standard deviation of the elastic parameters, this approach uses Monte-Carlo simulations and finite elements, where each simulation leads to an effective value of the property under investigation. The results are extended to investigate an influence of representative volume element (RVE). A comparison of the effective elastic stiffness of 2D and 3D models is also discussed.

**Keywords:** Random finite element method (RFEM), Representative volume element (RVE), Effective elastic properties, Homogenization

## 1 Introduction

The motivation of this work is to investigate the influence of porosity and void size on the stiffness of 3D geomaterials using a statistical approach. Even if the expected porosity of a site can be conservatively estimated, the location of the voids may be largely unknown such as in geological regions dominated by karstic deposits. This makes a statistical approach appealing. The work presented in this paper is developed from a study of 2D model homogenization of geomaterials containing voids by random fields and finite elements (Griffiths et al. 2012) and 3D model of random finite element method (Fenton and Griffiths, 2005). The classic problem of a homogenization on a micro-structure has long been of practical interest to engineers, because the macrostructure of a homogeneous material depends on a heterogeneous microstructure which varies spatially and may contains random voids. Many models have been conducted to determine effective elastic properties however 3D model will clearly be more realistic because the shape of voids in 2D model has infinite depth. The goal of homogenization is to predict the effective property of a heterogeneous material, where the effective value is defined as the property that would have led to the same response if the geomaterial had been homogeneous. A useful concept in this homogenization process is the representative volume element (RVE). An RVE is an element of the heterogenous material is large enough to represent the microstructure and it is small enough to achieve the efficient computational modeling (e.g. Liu, 2005; Zeleniakiene et al., 2005).

Since the concept of the RVE was first introduced by Hill (1963), several theoretical models have been proposed for dealing with scale effects. Hazanov and Huet (1994) derived results involving mixed boundary conditions, which located between the static and kinematic uniform boundary conditions for specimens smaller than the size of the RVE. The orthogonal mixed

boundary conditions were proposed in more details relating to the Hill principal (e.g. Hazanov and Amieur, 1995; Havanov, 1998; Khisaeva and Ostoja-Starzewski, 2006). Numerical methods such as the Finite Element Method (FEM) have been used to validate the RVE size of random heterogeneous materials. Kanit et al (2003) considered a minimal number of simulations relating to volume size and effective property while Zohdi and Wriggers (2001) and Ostoja-Starzewski (2006) considered the RVE size with a statistical computational approach. Although there are many models developed to investigate the effective properties of a material containing voids and the size of RVE, there is no model considered to be a “best micromechanical approach” for all problems (Bhm, 1998, 2013). See also the review of Torquato (2002), Kachanov (2005) and Klusemann and Svendsen (2009).

In this paper, the random finite element method (RFEM) (e.g. Fenton and Griffiths 2008), which combines finite element analysis with random field theory, will be used in conjunction with Monte-Carlo simulations, to examine the effective elastic properties of materials with randomly distributed voids. A 3D cube of material, discretized into a relatively fine mesh of 8-node hexahedron elements, forms the basis of the model. Random field theory will be used to generate a material containing in-tact material and voids with controlled porosity and size. The RFEM can vary the size of the voids through control of the spatial correlation length, and takes full account of element size in the random field, thus delivering statistically consistent values of the locally averaged properties (e.g. Fenton and Vanmarcke, 1990). For each simulation of the Monte-Carlo process, elements in the mesh are assigned either an in-tact stiffness value or a much lower stiffness value corresponding to a void. A deterministic analysis follows leading to effective values of the elastic parameters  $E$  and  $\nu$ . Monte-Carlo analyses are typically repeated numerous times until the output statistics of the effective elastic properties stabilize.

The first part of the paper investigates the size of the RVE for different input void properties. The second part of the paper investigates the statistics of the effective Young's modulus and Poisson's ratio in 3D as a function of porosity and void size, and compares results with numerical and analytical studies by other investigators. Effective properties in 3D are also compared with 2D results obtained in previous work (Griffiths et al. 2012).

## 2 Finite Element Model

The random finite element method (RFEM) (Fenton and Griffiths 2008) combines finite element methods and random field theory. In this paper, finite element analysis of a 3D cube of elastic material using 8 nodes hexahedron elements is combined with random field generation and Monte-Carlo simulations to model an elastic material containing voids. The goal is to develop output statistics of the effective Young's modulus and Poisson's ratio for different void sizes and porosity. Examples of the model which combines elastic material and voids are shown in Figure.1.

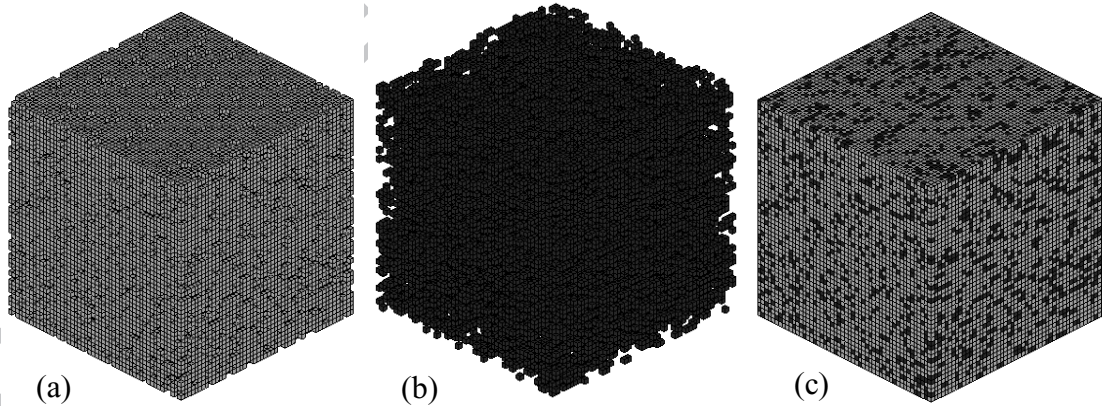


Figure 1 The 3D finite element model of ideal cubic blocks: (a) the solid material, (b) the voids, and (c) the combined model which show dark and light regions indicating voids and solid material respectively

The finite element mesh for this study consists of a cubic block of material of side length  $L = 50$  modeled by  $50 \times 50 \times 50$  8-node cubic elements of side length  $\Delta x = \Delta y = \Delta z = 1.0$ . Any consistent system of units could be combined with the dimensions and properties described in this paper. Since a mesh such as this involves rather large global matrices, equation solution in the runs described in this paper will be performed using a preconditioned conjugate gradient (PCG) technique with element-by-element products as described by Smith and Griffiths (2004) which avoids entirely the need to assemble the global stiffness matrix. The model in Figure 2 is subjected to a vertical force  $Q = L \times L$  on the top face leading to an average unit pressure on the top face of 1.0. The boundary conditions of the block involve the use of “tied freedom” that allow analysis of an “ideal” block and direct evaluation of the effective Young’s modulus and Poisson’s ratio. Tied freedoms are forced to move by the same amount in the analysis. The boundary conditions are such that the cubic block remains a regular hexahedron after deformation. Other methods may give similar outcomes (see the effects of tied freedom boundary condition from Huang et al., 2013). From this idea, the effective Young’s modulus and Poisson’s ratio easily be back-figured as will be described.

In particular, the boundary conditions are such that nodes on the base of the block can move only in the  $x - y$  plane. The back left and back right faces are constrained to move only in the  $y - z$  and  $z - x$  planes respectively. All  $z -$  freedoms on the top plane are tied, as are the  $y -$  freedoms on the front left plane and the  $x -$  freedoms on the front right plane. A consequence of these constraints is that the top surface remaining horizontal and the two front sides remaining vertical following deformation.

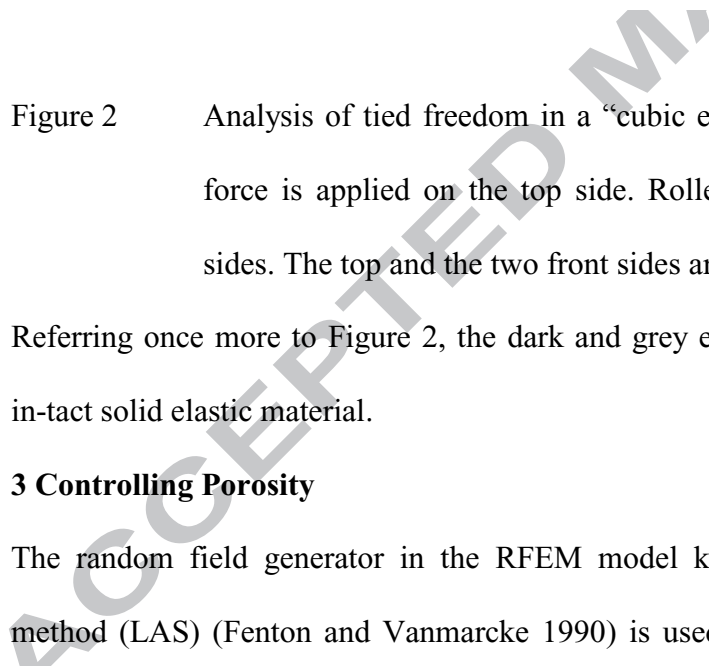


Figure 2 Analysis of tied freedom in a “cubic element test” model with voids. A vertical force is applied on the top side. Rollers are fixed at the bottom and two back sides. The top and the two front sides are tied.

Referring once more to Figure 2, the dark and grey elements represent, respectively, voids and in-tact solid elastic material.

Figure 2 Analysis of tied freedom in a “cubic element test” model with voids. A vertical force is applied on the top side. Rollers are fixed at the bottom and two back sides. The top and the two front sides are tied.

Referring once more to Figure 2, the dark and grey elements represent, respectively, voids and in-tact solid elastic material.

### 3 Controlling Porosity

The random field generator in the RFEM model known as the Local Average Subdivision method (LAS) (Fenton and Vanmarcke 1990) is used in this paper to model spatially varying voids properties. The general methodology has been applied successfully to model random variation of material (constitutive) properties which may be defined at the point (or micro-) scale. In finite element analysis, constant properties are typically assigned to each element, which means some account needs to be taken of the element size in relation to the spatial



correlation length. The larger the element, and the coarser the mesh, the greater the variance reduction. There is no avoiding mesh discretization errors, however local averaging at least reduces this source of error in a random materials by adjusting the statistical input parameters in a consistent way. In the current work, the local averaging effect is modest because we are using relatively fine meshes and random fields merely as a vehicle for modeling porosity and void size. The targeted mean porosity  $n$  is obtained by using the standard normal distribution shown in Figure 3.

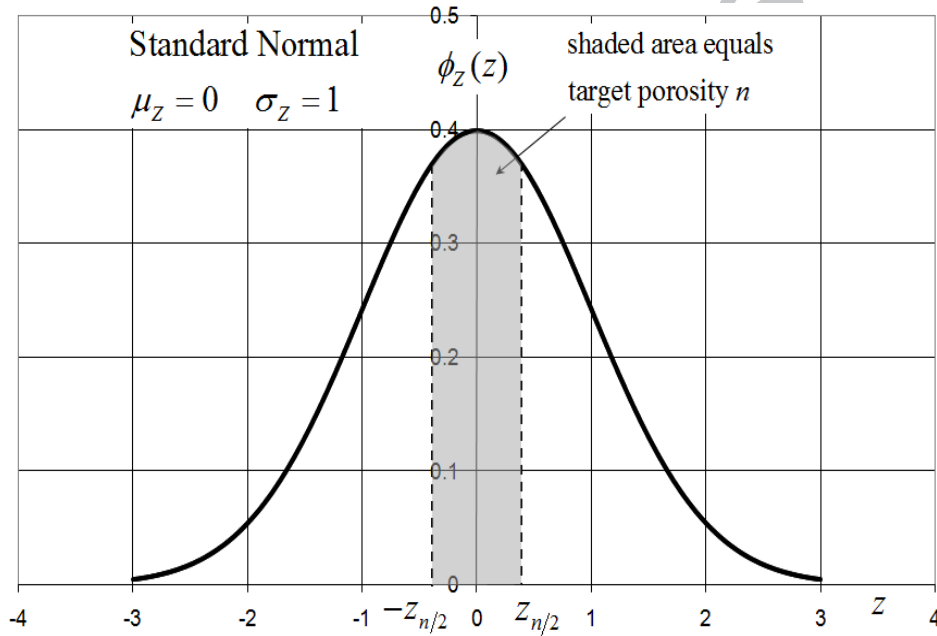


Figure 3 Target porosity area in standard normal distribution of random field. Any element assigned a random field value in the range  $|Z| > z_{n/2}$  is treated as intact material a Young's modulus and Poisson's ratio given by  $E_0 = 1$  and  $\nu_0 = 0.3$ , respectively

The RFEM takes a full account of element size in the random field generation and the method delivers statistically consistent values of the locally averaged properties. A single value of the random variable  $Z$  then will be generated for each element of the finite element mesh. Once the



standard normal random field values have been assigned to the mesh, cumulative distribution tables  $\Phi$  (suitably digitized in the software) are then used to estimate the value of the standard normal variable  $z_{n/2}$  for which

$$\Phi(z_{n/2}) - \Phi(-z_{n/2}) = n \quad (1)$$

where  $\Phi$  is the cumulative normal distribution function, and  $n$  is the target porosity .

as shown in Figure 3. Thereafter, any element assigned a random field value in the range  $|Z| > z_{n/2}$  is treated as intact material a Young's modulus and Poisson's ratio given by  $E_0 = 1$  and  $\nu_0 = 0.3$ , respectively, while any element where  $|Z| \leq z_{n/2}$  is treated as a void element with an assigned Young's modulus of  $E = 0.01$  (100 times smaller than the surrounding intact material). There are only two different materials modeled in the finite element analysis. Each void is modeled explicitly as a material with significant lower stiffness than the intact material. As can be seen in Figure 4, for the case when  $n = 0.2$ , the results show a small influence due to the selected Young's modulus of void elements. In the current work, a void stiffness which is one hundred times less than the intact material gives reasonable (and stable) results.

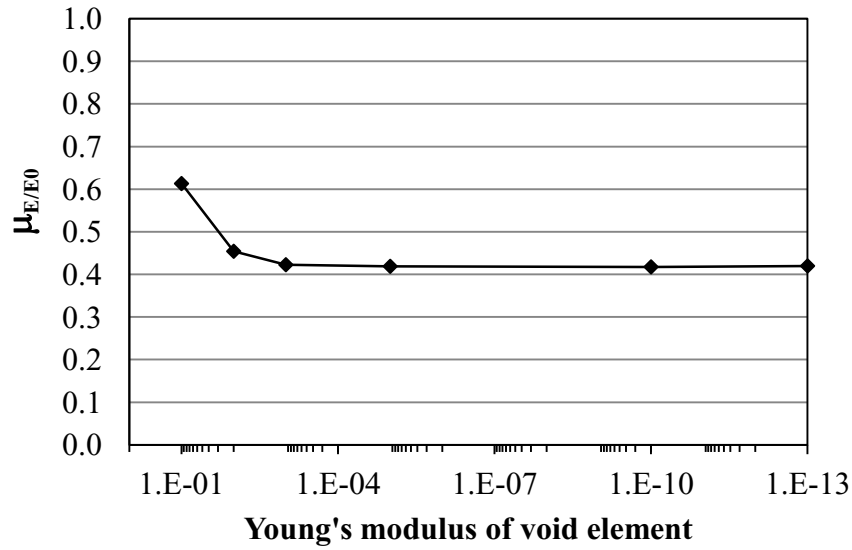


Figure 4 Influence of void element stiffness on the mean effective Young's modulus.

Intact material stiffness  $E_0 = 1$

The nature of random fields is that the mean porosity is under the user's control, but the porosity of each individual simulation processed by the Monte-Carlo method will vary from one simulation to the next. Figure 3 shows the methodology for generating the target porosity, whereas Figure 5 shows a typical simulation of the Monte-Carlo process in which the histogram indicates the frequency of standard normal values assigned to each element. It can be seen that the simulation gives a porosity of 0.274. This is particularly noticeable when modeling random fields with higher spatial correlation length, in which some individual simulations may display significantly higher or lower porosities than the target value.

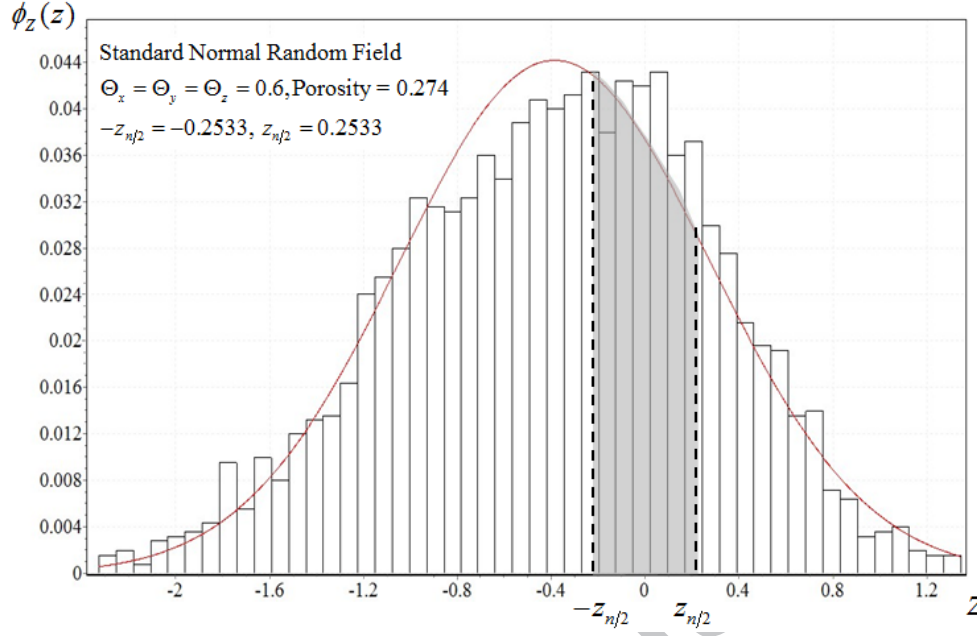


Figure 5 A single simulation of the random field assigned to the mesh. The porosity of each individual simulation processed by the Monte-Carlo method will vary between the simulations

The influence of randomly distributed voids on the elastic properties of isotropic media (i.e., intact material is isotropic) is investigated in this work where both the voids and the intact material are assigned isotropic properties at the micro-level. It is recognized that there are cases where the intact materials are anisotropic for various reasons (i.e., if micro scale is small enough, most materials are anisotropic), however this is beyond the scope of the present work. Even though an individual simulation may *appear* heterogenous (and even anisotropic), after a sufficient number of Monte-Carlo simulations, the overall statistical response is isotropic, i.e. on the average the void shapes would tend to spheres.

#### 4 Controlling of Void Size

As mentioned previously, two materials with the same average porosity could have quite different void sizes. One model could have frequent small voids, while the other could have less

frequent larger voids. The void size in this study is controlled by the random field spatial correlation length  $\theta$  which incorporates a “Markov” spatial correlation structure as follows

$$\rho(\tau) = \exp(-2|\tau|/\theta) \quad (2)$$

where  $\rho$  = the correlation coefficient;  $|\tau|$  = absolute distance between points in the field; and  $\theta$  = scale of fluctuation or spatial correlation length. Larger values of  $\theta$  will lead to larger voids and vice versa

The Markov equation delivers a spatial correlation that reduces exponentially with distance. For example, from Eq. (2),  $\tau < \theta$ , the correlation coefficient  $\rho > 0.13$ . In the current study, the range of  $\rho$  varies from 0 to 1. Points close together are strongly correlated and therefore likely to belong to the same void. In the limiting case of  $\theta \rightarrow 0$ , the random field value changes rapidly from point to point delivering numerous small voids. At the other extreme as  $\theta \rightarrow \infty$ , the random on each simulation becomes increasingly uniform with some simulations representing entirely in-tact material and other consisting entirely of voids.

For example as shown in Figure 6, the models show typical simulations of different void clustering for two materials with the same mean porosity.

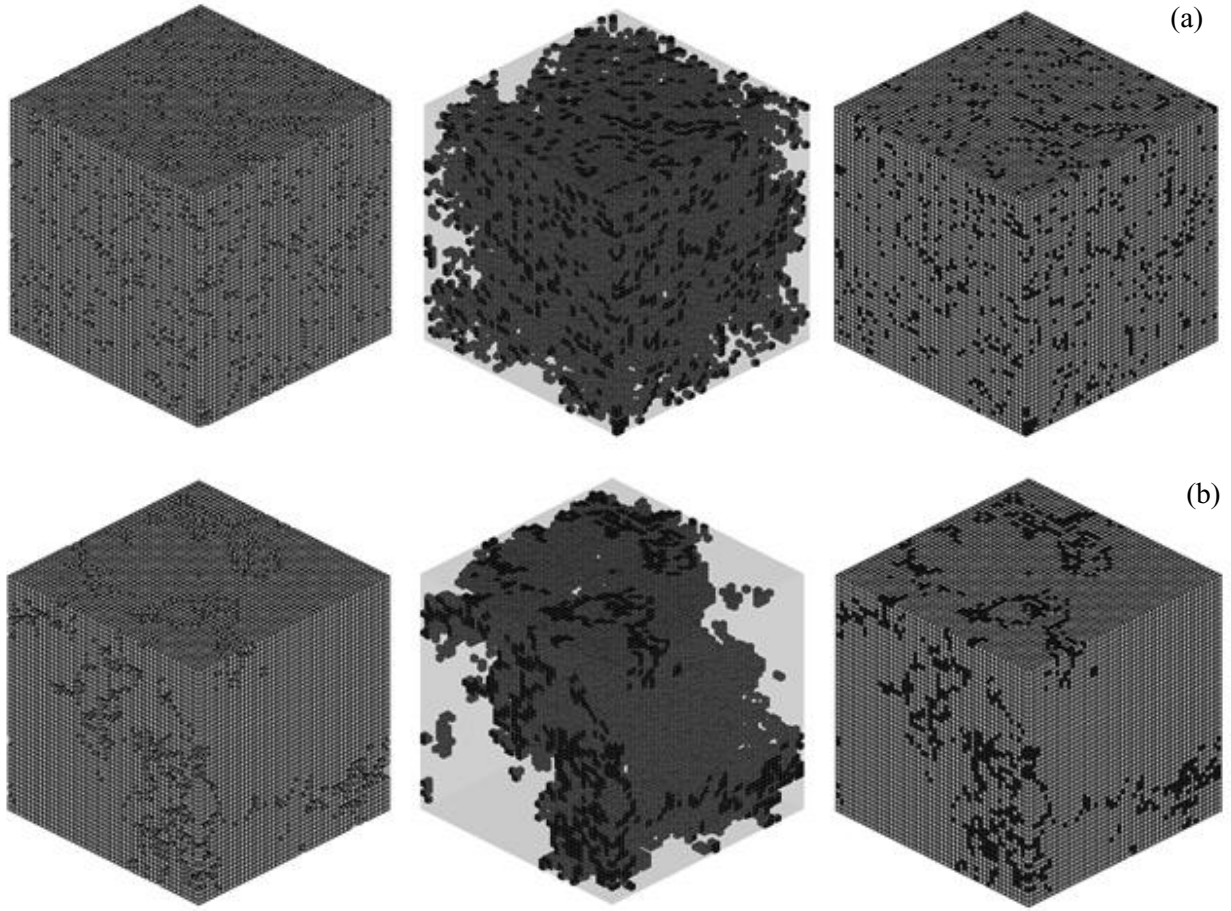


Figure 6 Typical simulations showing generation of voids at (a) low and (b) high spatial correlation lengths  $\theta$  ( $n = 0.1$  in both cases)

### 5 Monte-Carlo Simulations

A “Monte-Carlo” process is combined with the RFEM and repeated until stable output statistics are achieved. The primary outputs from each elastic analysis are the vertical and horizontal deformations of the block  $\delta_z$ ,  $\delta_x$  and  $\delta_y$ . Although each simulation uses the same  $\theta$  and  $n$ , the spatial location of the voids will be located in different places. In some cases, the voids may be located just below the top of the block leading to a relatively high  $\delta_z$ . While in others, the voids may be buried in the middle of the block leading to a relatively low  $\delta_z$ . Following each

simulation, the computed displacements  $\delta_z$ ,  $\delta_x$  and  $\delta_y$  are converted into the “effective” values of Young’s modulus and Poisson’s ratio as follows.

Based on Hooke’s law,

$$\begin{aligned}\varepsilon_x &= \frac{1}{E}(\sigma_x - \nu(\sigma_y + \sigma_z)) \\ \varepsilon_y &= \frac{1}{E}(\sigma_y - \nu(\sigma_z + \sigma_x)) \\ \varepsilon_z &= \frac{1}{E}(\sigma_z - \nu(\sigma_x + \sigma_y))\end{aligned}\quad (3)$$

Given that  $L$  is the side length of cubic block, and assume stress boundary conditions

$$\sigma_x = 0.0, \sigma_y = 0.0, \sigma_z = -Q/L^2 \quad (4)$$

$$\varepsilon_x = \frac{\delta_x}{L}, \varepsilon_y = \frac{\delta_y}{L}, \varepsilon_z = \frac{\delta_z}{L} \quad (5)$$

hence after substitution into equation (3), the effective elastic properties can be written as

$$E = \frac{Q}{L\delta_z} \quad (6)$$

$$\nu_x = \frac{\delta_x}{\delta_z} \quad (7)$$

$$\nu_y = \frac{\delta_y}{\delta_z} \quad (8)$$

where  $E$  = the effective elastic Young’s modulus,  $Q$  = loading at the top side,  $\nu_x$  and  $\nu_y$  = the effective Poisson’s ratios based on the displacement in the  $x$  – and  $y$  – directions respectively.

In each simulation, the effective Young’s modulus is normalized as  $E/E_0$  by dividing by the intact Young’s modulus  $E_0$ . In the current study, following some numerical experiments as shown in Figure 7, it was decided that 1000 simulations for each parametric combination would

deliver reasonably repeatable results. In this study, we have expressed the spatial correlation length in dimensionless form.

$$\Theta = \frac{\theta}{L} \quad (9)$$

where  $L$  is the width of the loaded element ( $L = 50$ )

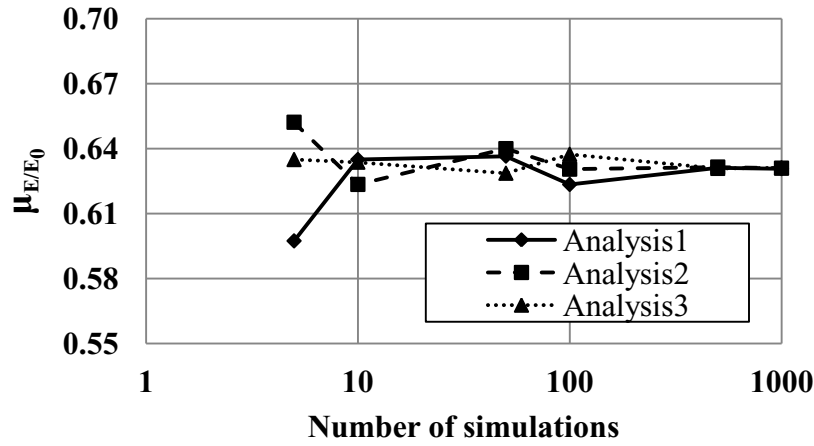


Figure 7 Sensitivity of the mean effective young's modulus as a function of the number of simulations for  $n = 0.2$  and  $\Theta = 0.4$ . It was decided that 1000 simulations would deliver reasonably repeatability.

## 6 Representative Volume Element

An RVE is an element of the heterogenous material is large enough to represent the microstructure and it is small enough to achieve the efficient computational modeling, we consider the RVE of four cases using the random field 3D finite element model, as follows



Table 1 Different input void properties

Case	$n$	$\Theta$
1	0.2	0.2
2	0.2	0.7
3	0.7	0.2
4	0.7	0.7

The statistical results of each set of Monte-Carlo simulations are shown in Figure 8.

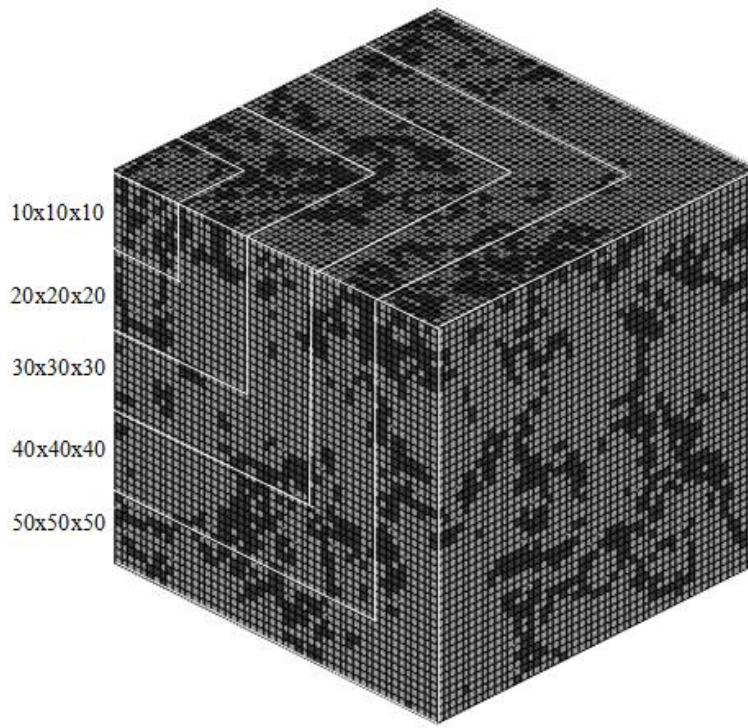
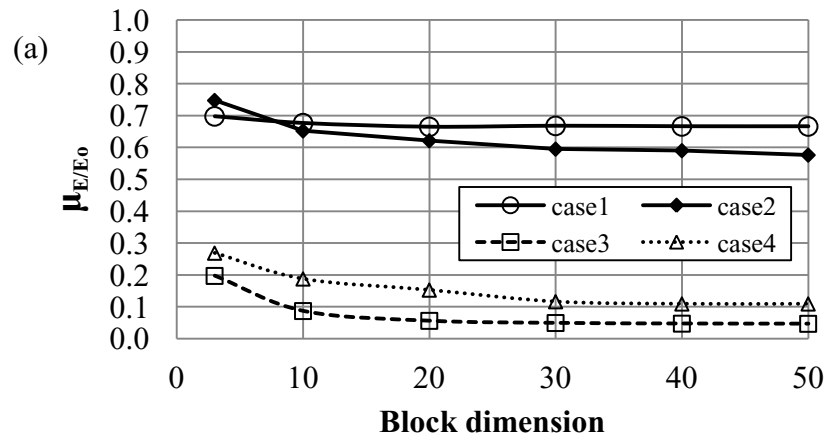


Figure 8 Different block sizes for computing the effective elastic properties of a material with random voids

Figure 8 shows a sequence of five blocks contained within and including the largest block of  $50 \times 50 \times 50$  cubic elements. The different block sizes will indicate the optimal RVE for the given input conditions. When the RVE is “big enough”, we expect the standard deviation of the

effective Young's modulus to be reduced and its mean essentially constant as shown in Figures 9(a) and 9(b).

While the mean values plotted in Figure 9(a) are fairly constant for different block sizes, it could be argued that the block size of  $20 \times 20 \times 20$  led to essentially constant values for the low  $\Theta$  cases (1 and 3), while a larger block, say  $30 \times 30 \times 30$  would be needed for stable mean values with the larger  $\Theta$  cases (2 and 4). The standard deviation shown in Figure 9(b) displays more variability with block size and tends to zero as the blocks get bigger, but at a slower rate for higher values of  $\Theta$ . In both Figures 9, it is noted that the influence of  $\Theta$  on block statistics is greater than that of  $n$ . The RVE depends more on spatial correlation length than porosity.



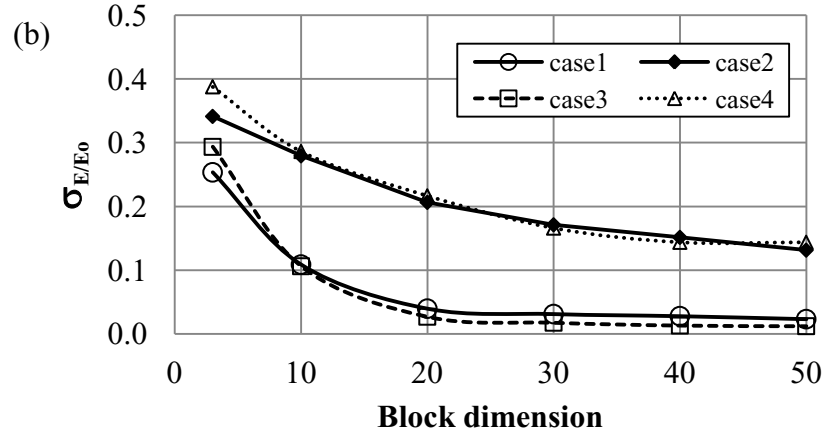
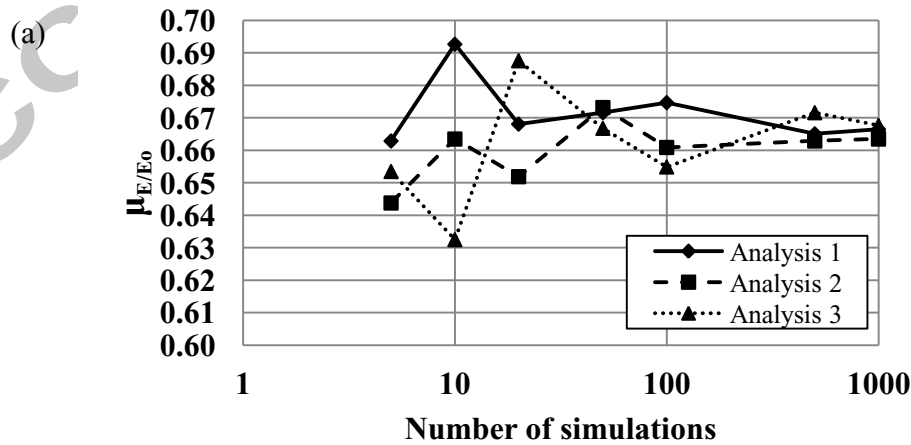


Figure 9 Effective Young's modulus (a) mean and (b) standard deviation following 1000 simulations for different block sizes

If the block is large enough, each simulation would give an identical result. This effect is shown in Figure 10 where the variation of mean Young's modulus is plotted against the number of Monte-Carlo simulations corresponding to  $20 \times 20 \times 20$  and  $50 \times 50 \times 50$  blocks for three repeated analyses. For the smaller  $20 \times 20 \times 20$  block, the effective Young's modulus takes at least 1000 simulations to stabilize in Figure 10 (a), while the larger  $50 \times 50 \times 50$  block settles down in around 500 in Figure 10 (b). The choice of the RVE should be put in the context of the application being considered and accuracy required. Further results relating to  $\Theta$  have not been included here.



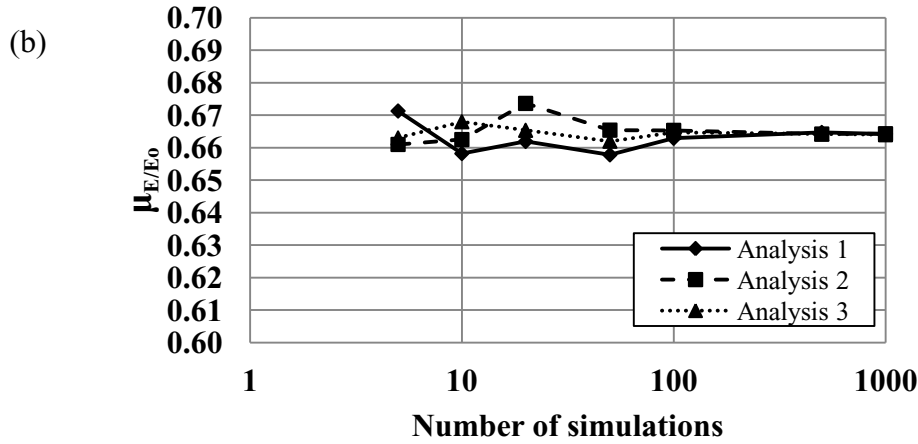


Figure 10 Comparison of the number of simulations for convergence with different block sizes: (a)  $20 \times 20 \times 20$  and (b)  $50 \times 50 \times 50$  with  $n=0.2$  and  $\Theta=0.2$

Although the finite element programs have the ability to model anisotropic random fields, and therefore anisotropic void distributions, none was considered in the current work. The void modeling was strictly isotropic. It is true that while a typical simulation of the Monte-Carlo process may appear to generate anisotropic void distributions, this is statistically insignificant. If the shape of voids was measured in a systematic way and averaged over a large number of simulations, the *average* void shape in the current work would be spherical, with a diameter dictated by the spatial correlation length. Figure 8 is about the investigation of the size of RVE for an isotropic medium. If the global response is truly anisotropic, more elastic constants than just one  $E$  and one  $\nu$  would be needed, which would be beyond the scope of the present study.

In order to confirm the statistical isotropy of the model, loading was applied in three different directions to the block shown in Figure 2. Following Monte-Carlo simulations, it can be seen that the mean Young's modulus was essentially the same regardless of the direction of loading as shown in Figure 11. The standard deviation of Young's modulus was similarly insensitive to loading direction.

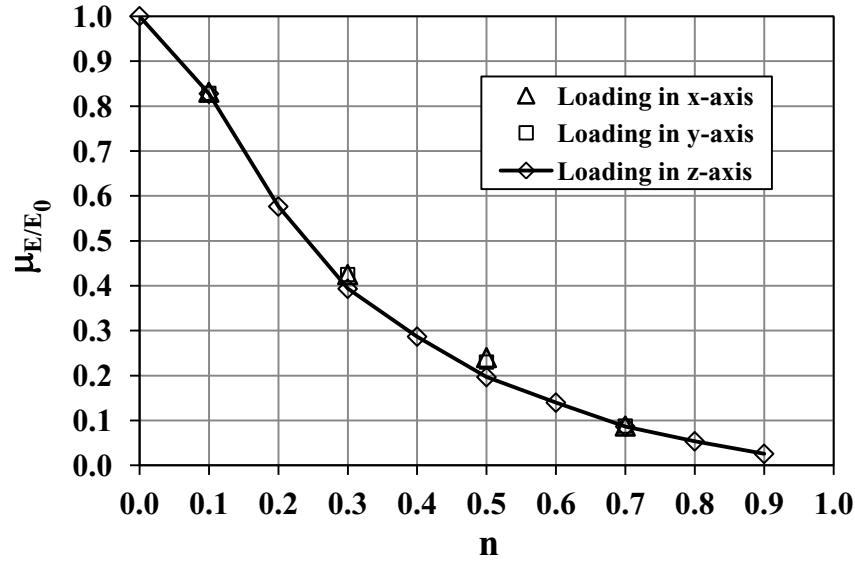


Figure 11 Comparison of the mean effective Young's modulus obtained from three different directions of loading. ( $\Theta = 1.0$  for all cases).

## 7 Results of RFEM

Following each set of 1000 Monte-Carlo simulations, the mean and standard deviation of the normalized effective Young's modulus were computed for a range of parametric variations of  $n$  and  $\Theta$ , with results shown in Figures 12 and 13, respectively.

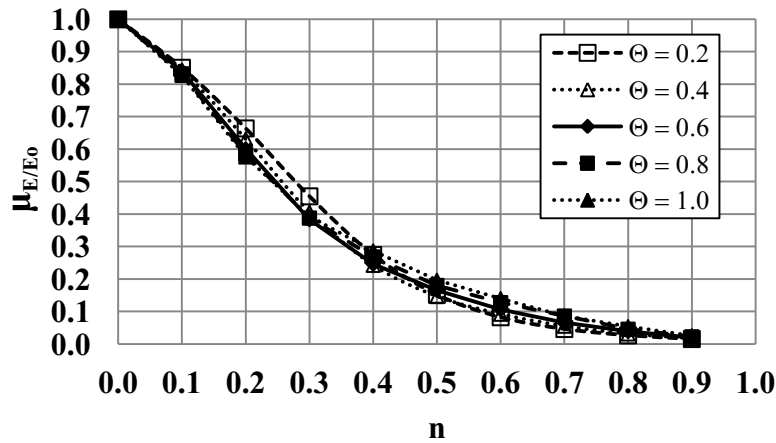


Figure 12  $\mu_{E/E_0}$  vs.  $n$  for  $0.2 \leq \Theta \leq 1.0$

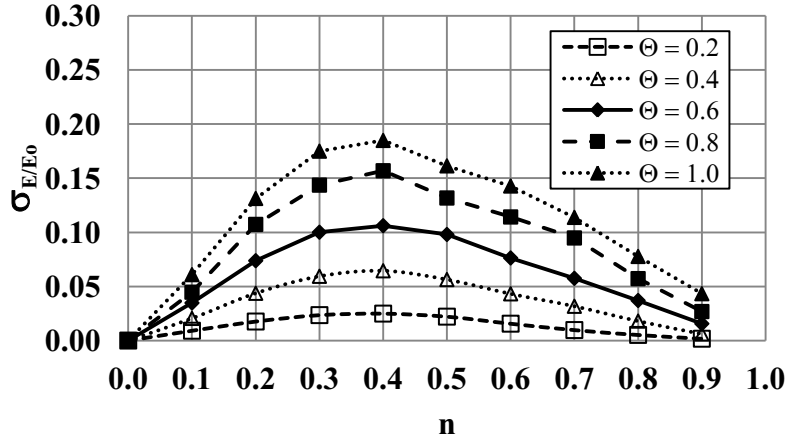


Figure 13  $\sigma_{E/E_0}$  vs.  $n$  for  $0.2 \leq \Theta \leq 1.0$

It can be noted from Figure 12 that the mean normalized effective Young's modulus drops towards zero with increasing porosity  $n$  and that  $\Theta$  does not have much influence. Figure 13 shows that  $\Theta$  has more influence on the standard deviation of the effective Young's modulus  $\sigma_{E/E_0}$ . The standard deviation values as  $n \rightarrow 0$  (intact stiffness material) and  $n \rightarrow 1$  (zero stiffness material) show very low variance since almost all simulations are the same and model essentially uniform material. The standard deviation was observed to reach a maximum value at around  $n \approx 0.4$ .

The result obtained from Equations 7 and 8 for the effective Poisson's ratio were in good agreement as expected for the range of  $n$  and  $\Theta$  considered. In the isotropic material model, the mean and standard deviation of the two Poisson's ratios were essentially identical after Monte-Carlo simulation; however the results are based on an average to account for any small differences. The plots shown in Figures 14 and 15 give the mean and standard deviation of the effective Poisson's ratio. Figure 14 shows that the mean effective Poisson's ratio  $\mu_v$  displays a minimum at around  $n = 0.5$ . On the other hand, as shown in Figure 15, the standard deviation

values of Poisson's ratio  $\sigma_v$  displays a maximum at  $n=0.7$ . For all values of  $\Theta$  considered however, the standard deviations were quite small.

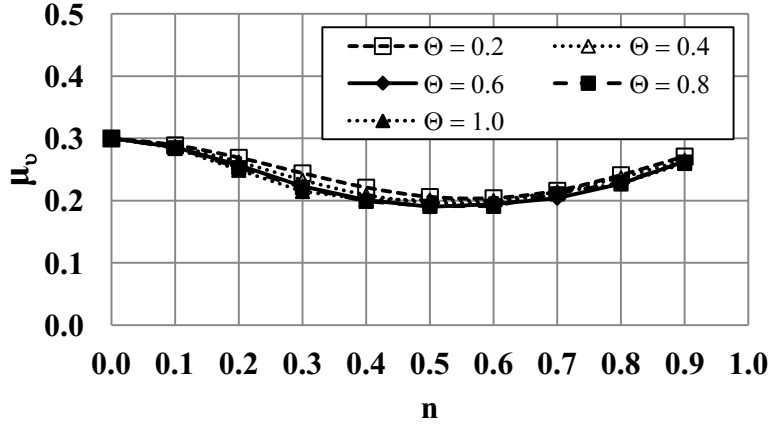


Figure 14  $\mu_v$  vs.  $n$  for  $0.2 \leq \Theta \leq 1.0$

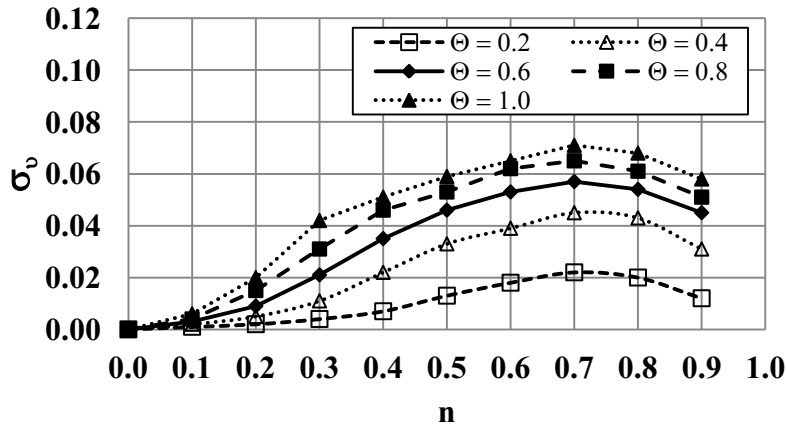


Figure 15  $\sigma_v$  vs.  $n$  for  $0.2 \leq \Theta \leq 1.0$

Although this paper has focused on Young's modulus and Poisson's ratio, other stiffness moduli may be of interest depending on the context. Figure 16 combines results from Figures 12 and 14 to show the variation of the mean effective shear modulus and bulk modulus using Eqns. (10-11). They display a similar trend to that observed for Young's modulus.

$$\mu_k = \frac{\mu_E}{3(1-2\mu_v)} \quad (10)$$



$$\mu_s = \frac{\mu_E}{2(1 + \mu_v)} \quad (11)$$

where  $\mu_k$  = the mean effective bulk modulus,  $\mu_s$  = the mean effective shear modulus.

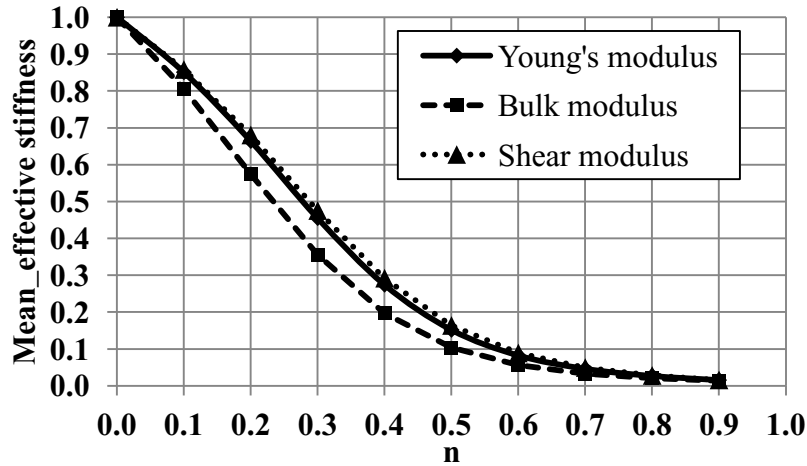


Figure 16 Mean effective values vs.  $n$  using  $\Theta = 0.2$

## 8 Computer Resources and Timings

A desktop with an Inter Core i7-2600 CPU @ 3.4 Ghz Ram: 8 GB was used to obtain all results presented in this paper. Figure 17 shows the CPU time used for different block sizes. The results show that the CPU time depends more on porosity than spatial correlation length. At a  $50 \times 50 \times 50$  mesh, the CPU time for the high porosity case was about 200 hours, while for a low porosity it was more like 90 hours. The reason for this discrepancy is thought to be the slower convergence observed in the iterative solvers when there is more variability present in the stiffness matrices with high void content. The results of sensitivity studies with different levels of mesh refinement are shown in Figures 18 (a) and 18 (b) for the case when  $\Theta = 0.2$ . The results of  $50 \times 50 \times 50$  mesh provides a reasonable mesh density for investigating the role of random voids in this study.

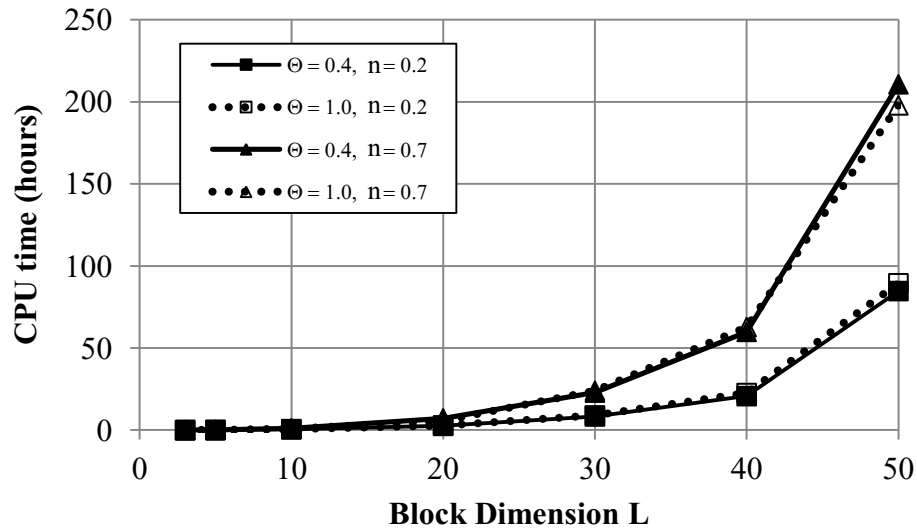
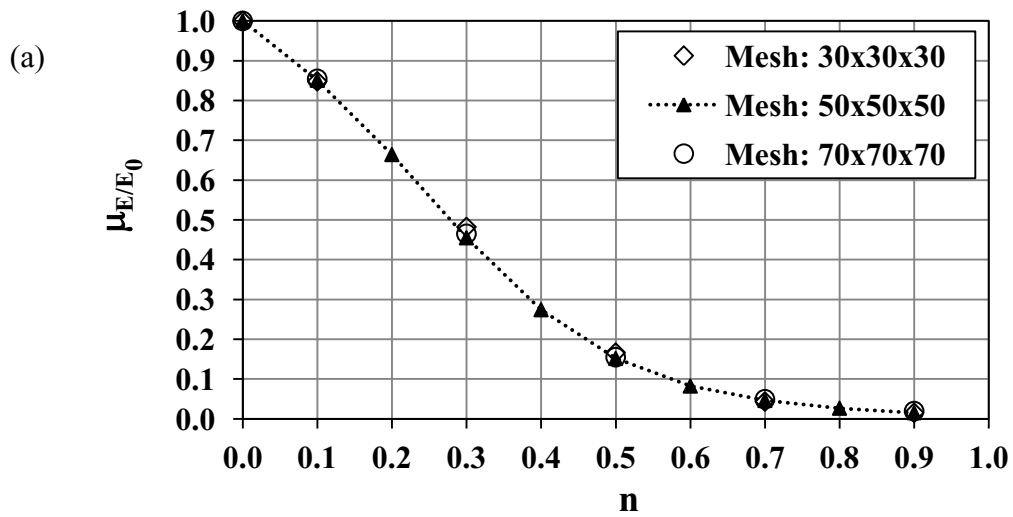


Figure 17 CPU timing for different block sizes with 1000 simulations



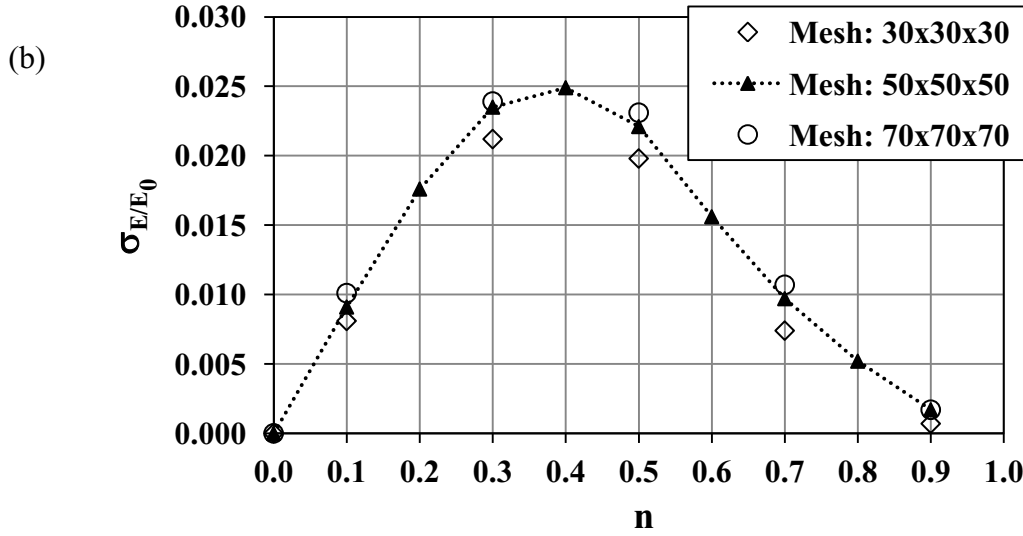


Figure 18 Influence of mesh refinement on (a) mean effective stiffness and (b) standard deviation of effective stiffness using  $\Theta = 0.2$

### 9 Comparisons of 2D and 3D Porosity Models

The difference between effective properties of 2D and 3D models have been investigated by a number of other researchers (e.g. Meille and Garboczi, 2001; Wiederkehr et al., 2010; Bobzin et al., 2012). Their works were based on 2D cross-sectional images created from 3D models however a different approach is used in the current work. The 3D results from the current study using  $\Theta = 0.6$  are compared with 2D (plane strain) for the same spatial correlation length as published previously by Griffiths et al. 2012 in Figure 19. The mean normalized effective Young's modulus in 3D is obviously higher than in 2D for the same porosity. A direct comparison between 2D and 3D may not be justified, however, because voids in 2D (plane strain) are like “tunnels” that continue indefinitely into the 3<sup>rd</sup> dimension, while voids in 3D are isotropic, finite in size, and fully contained within the surrounding material. Thus, it might be explained that the 2D model is actually a 3D model with an infinite spatial correlation length in the 3<sup>rd</sup> direction.

From Figure 19, it has been noted that the empirical relationship

$$n_{3D} = (n_{2D})^{2/3} \quad (12)$$

can be used as an approximate guide to the porosities in 2D and 3D that result in similar equivalent stiffness. The empirical relationship is also shown plotted on Figure 19 and it can be seen that agreement with actual 3D results is better for higher porosities.

For example, a 2D porosity of 0.3 gives a mean normalized effective Young's modulus of about 0.20. From Equation 12 the porosity in 3D that would lead to a similar stiffness would be 0.45.

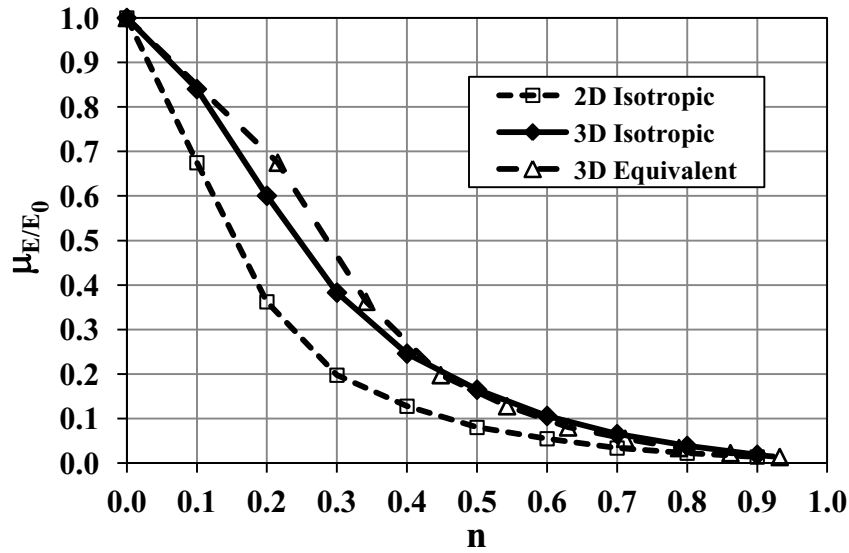


Figure 19 Comparison of the mean effective Young's modulus obtained from 2D and 3D RFEM models. ( $\Theta = 0.6$  for both models).

More sophisticated empirical relations can be developed, including effects of anisotropy, but this is beyond the scope of the present work.

### 10 Comparisons with 3D RFEM and Other Results

The theoretical results based on the Generalized Self Consistent Method of Christensen and Lo (1979) and the numerical results based on the single-cut GRF model of Roberts and Garboczi (2002) are compared in Figure 20, with results from the current study using  $\Theta = 0.6$  from Figure

10. The Generalized Self Consistent Method involved embedding an inclusion phase directly into an infinite medium. It was demonstrated that the method could also solve the spherical inclusion problem. The single-cut GRF model assigns a random number to each point in space. From Figure 20, it can be observed that the current method gives similar values of the mean effective Young's modulus to those given by the theoretical and numerical methods for all values of  $n$ . The theoretical studies based on the Voigt and Reuss bounds and Hashin-Shtrikman bounds (1963) have long been of interest to estimate the effective properties (See also Gross and Seelig, 2011). From the energetic principle of effective properties, an upper bound and lower bound solutions would be obtained, respectively, if the minimum of potential and complementary energetic principle are used. The Voigt and Reuss bounds use the porosity to approximate the effective properties. The effective bulk modulus by Voigt and Reuss bounds can be estimated as

$$K_{\text{Voigt}} = (1-n)K_0 + (n)K_{\text{void}} \quad (13)$$

$$K_{\text{Reuss}} = \frac{K_0 K_{\text{void}}}{(1-n)K_{\text{void}} + (n)K_0} \quad (14)$$

where  $n$  = target porosity and  $K_0$ ,  $K_{\text{void}}$  are the bulk modulus of material and void, respectively.

The Hashin-Shtrikman (HS) approach, which is a closer bounds between upper and lower bounds for two phase materials than the Voigt and Reuss bounds, can be estimated for an isotropic material as follows.

$$K_{\text{HS\_lower}} = K_{\text{void}} + (1-n) \left[ \frac{1}{K_0 - K_{\text{void}}} + \frac{3(n)}{3K_{\text{void}} + 4G_{\text{void}}} \right]^{-1} \quad (15)$$

$$K_{\text{HS\_upper}} = K_0 + (n) \left[ \frac{1}{K_{\text{void}} - K_0} + \frac{3(1-n)}{3K_0 + 4G_0} \right]^{-1} \quad (16)$$

$$G_{HS\_lower} = G_{void} + (1-n) \left[ \frac{1}{G_0 - G_{void}} + \frac{6(n)(K_{void} + 2G_{void})}{5G_{void}(3K_{void} + 4G_{void})} \right]^{-1} \quad (17)$$

$$G_{HS\_lower} = G_0 + (n) \left[ \frac{1}{G_{void} - G_0} + \frac{6(1-n)(K_0 + 2G_0)}{5G_0(3K_0 + 4G_0)} \right]^{-1} \quad (18)$$

where  $n$  = target porosity.  $K_0$ ,  $K_{void}$  are the bulk modulus of material and void, respectively.  $G_0$ ,  $G_{void}$  are the shear modulus of material and void, respectively.

The results of mean effective bulk modulus from Figure 16 are compared with the theoretical studies based on the upper and lower bounds of Voigt and Reuss approximations and Hashin-Shtrikman (HS) bounds in Figure 21. It can be observed that the values of the normalized effective bulk modulus ( $K^*$ ) from the current work lie in between the results given by the Voigt and Reuss bounds and Hashin-Shtrikman bounds for all values of  $n$ .

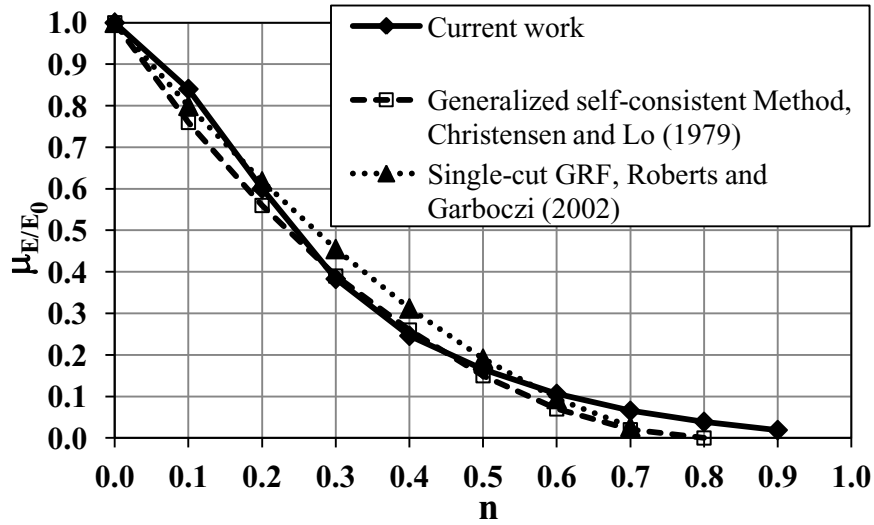


Figure 20 Comparison of the effective Young's modulus obtained from 3D RFEM and other approaches

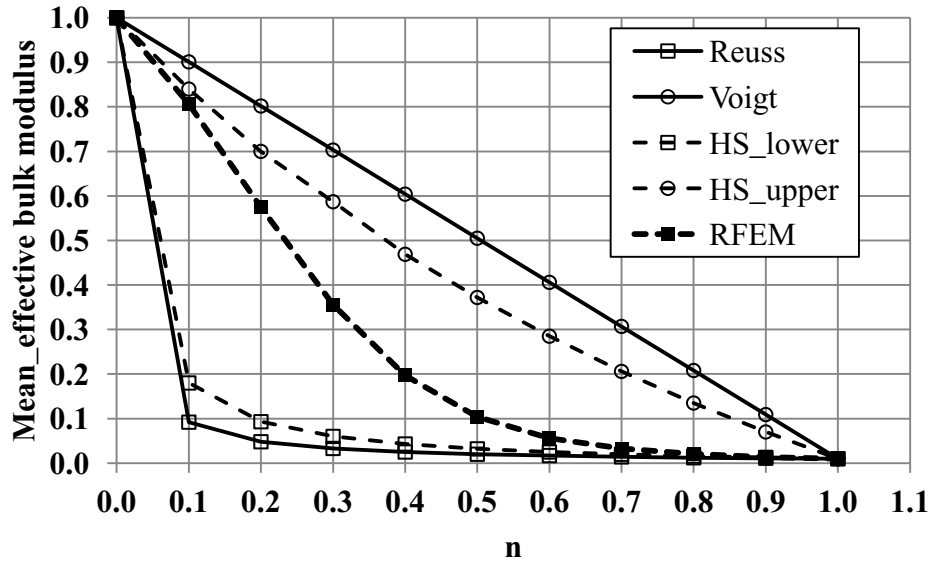


Figure 21 Comparison of the normalized effective bulk modulus ( $K^*$ ) obtained from 3D RFEM with the Voigt-Reuss bounds and Hashin-Shtrikman (HS) bounds

## 11 Concluding remarks

A 3D RFEM with “tied freedoms” has been used in this study to investigate the influence of porosity and void size on homogenized elastic properties  $E$  and  $\nu$ . It was observed that while porosity had a significant effect on both the mean and standard deviation of  $E$  and  $\nu$ , the void size had little influence on the mean but more influence on the standard deviation. The study also investigated the RVE needed to capture the essential properties of a heterogeneous material containing voids. It was found that for the same porosity, the larger the size of the voids, the greater the size of the RVE. Finally, the paper presented favorable comparisons of the effective elastic properties in 3D with those obtained analytically and numerically by other investigators. In addition, when the 3D results were compared with 2D obtained by the authors in a previous study, it was found that the effective elastic stiffness was consistently greater in 3D than in 2D.

The benefits of RFEM will become more apparent in the analysis of heterogeneous materials (including voids) that have no clear analytical alternative. For example, stratified materials in



which the porosity of each layer is different. The method also opens the ability to make probabilistic statements about engineering performance.

### Acknowledgement

The authors wish to acknowledge the support of (i) the Royal Thai Government, (ii) NSF grant CMMI-0970122 on “GOALI: Probabilistic Geomechanical Analysis in the Exploitation of Unconventional Resources”

### References

1. Bobzin, K., Kopp, N., Warda, T., and Ote, M., 2012. Determination of the effective properties of thermal spray coating using 2D and 3D models, *Journal of thermal spray technology*. Vol. 21(6). December 2012. JTTEE5 21:1269-1277, ASM International.
2. B hm, H.J., 1998, 2013. A short introduction to basic aspects of continuum micromechanics, TU Wien, Vienna.
3. Christensen R.M. and Lo K.H., 1979. Solutions for effective shear properties in three phase sphere and cylinder models, *J Mech Phys Solids*, 27:315-30.
4. Fenton G.A. and Griffiths D.V., 2005. Three-Dimension Probabilistic Foundation Settlement. *J. Geotech. Geoenviron. Eng.*, 131(2), 232-239.
5. Fenton G.A. and Griffiths D.V., 2008. Risk Assessment in Geotechnical Engineering, John Wiley & Sons, Hoboken, NJ.
6. Fenton G.A. and Vanmarcke E.H., 1990. Simulation of random fields via local average subdivision, *J Eng. Mech.*, vol.116, no.8, pp. 1733-1749

7. Griffiths D.V. Paiboon J. Huang J. and Fenton G.A., 2012. Homogenization of geomaterials containing voids by random fields and finite elements. *International Journal of Solids and Structures*, 49:2006-2014
8. Gross, D. and Seelig, T., 2011. Micromechanics and homogenization. *Fracture mechanics, mechanical engineering series*, pp 229-299
9. Hashin Z., and Shtrikman S., 1963. A variational approach to the theory of the elastic behavior of multiphase materials. *J.Mech.Phys.Sol.*, 11:127–140
10. Hazanov, S. and Huet, C. 1994, Order Relationships for Boundary-Conditions Effect in Heterogeneous Bodies Smaller Than the Representative Volume. *Journal of the Mechanics and Physics of Solids*, 42(12): p. 1995-2011.
11. Hazanov, S. and Amieur, M. 1995, On Overall Properties of Elastic Heterogeneous Bodies Smaller Than the Representative Volume. *International Journal of Engineering Science*, 33(9): p.1289-1301
12. Hazanov, S., 1998. Hill condition and overall properties of composites. *Archive of Applied Mechanics*, 68(6): p.385-394
13. Hill R., 1963. Elastic properties of reinforced solids: some theoretical principles, *J. Mech. Phys. Solids*, 11, 357-372
14. Huang, J.S., Krabbenhoft, K., Lyamin, A., 2013. Statistical homogenization of elastic properties of cement paste based on X-ray microtomography images. *Int. J. Solids Structure* 50: p. 699-709
15. Kachanov, M., Sevostianov, I., 2005 On quantitative characterization of microstructures and effective properties. *Int. J. Solids Struct.*, 42, pp. 309-336

16. Kanit, T., Forest, S., Galliet, I., Mounoury, V., and Jeulin, D., 2003 Determination of the size of the representative volume element for random composites: statistical and numerical approach. *International Journal of Solids and Structures*. 40(13-14): p.3647-3679
17. Khisaeva, Z.F., Ostoja-Starzewski, M., 2006. On the size of RVE in finite elasticity of random composites. *Journal of Elasticity* 85 (2), 153–173.
18. Klusemann, B. and Svendsen, B. 2009. Homogenization methods for multi-phase elastic composites Comparisons and Benchmarks, *Technische Mechanik*, 30, 4, (2010), 374-386
19. Liu, C., 2005. On the minimum size of representative volume element: an experimental investigation. *Exp. Mech.* 45 (3), 238–243
20. Meille, S. and Garboczi, E.J., 2001. Linear elastic properties of 2-D and 3-D models of porous materials made from elongated objects, *Mod. Sim. Mater. Sci. and Eng.* 9 (5), 371-390
21. Ostoja-Starzewski, M. 2006, Material spatial randomness: From statistical to representative volume element. *Probabilistic Engineering Mechanics*, 21(2): p. 112-132
22. Roberts, A.P. and Garboczi, E.J., 2002. Computation of the linear elastic properties of random porous materials with a wide variety of microstructure, *Proc. Royal Soc. of London*, 458 (2021), 1033-1054
23. Smith I.M. and Griffiths D.V., 2004. *Programming the finite element method*, John Wiley and sons, Chichester, New York, 4<sup>th</sup> edition
24. Torquato S., 2002. *Random Heterogeneous Materials: Microstructure and Macroscopic properties*. Springer-Verlag, NY

25. Wiederkehr, T., Klusemann, B., Gies, D., Muller, H., and Svendsen, B., 2010. An image morphing method for 3D reconstruction and FE-analysis of pore networks in thermal spray coating. Computational Materials Science 47: p.881-889
26. Zeleniakiene, D. Griskevicius, P. and Leisis, V., 2005. The comparative analysis of 2D and 3D microstructural models stresses of porous polymer materials. ISSN 1392-1207. MECHANIKA, Nr.3(53)
27. Zohdi, T.I. and Wriggers, P., 2001. Aspects of the computational testing of the mechanical properties of microheterogeneous material samples. International Journal for Numerical Methods in Engineering. 50(11): p.2573-2599

#### NOTATION

$E$	Effective Young's modulus
$E_0$	Young's modulus of intact material
$K_0$	Bulk modulus of intact material
$K_{void}$	Bulk modulus of void
$K^*$	Normalized bulk modulus
$G_0$	Shear modulus of intact material
$G_{void}$	Shear modulus of void
$\Delta x$	Element width
$\Delta y$	Element height
$\Delta z$	Element depth
$L$	Width and height of block
$n$	porosity
$n_{2D}$	porosity of 2D
$n_{3D}$	porosity of 3D
$Q$	Vertical force
$x, y, z$	Cartesian coordinates

$Z$	Random variable
$z_{n/2}$	Value of the standard normal variable
$\gamma$	Variance reduction due to local averaging
$\sigma_x$	Normal stress in $x$ direction
$\sigma_y$	Normal stress in $y$ direction
$\sigma_z$	Normal stress in $z$ direction
$\varepsilon_x$	Normal strain in $x$ direction
$\varepsilon_y$	Normal strain in $y$ direction
$\varepsilon_z$	Normal strain in $z$ direction
$\delta_x$	Deformation in $x$ direction
$\delta_y$	Deformation in $y$ direction
$\delta_z$	Deformation in $z$ direction
$\theta$	Spatial correlation length (dimensional)
$\Theta$	Spatial correlation length (non-dimensional)
$\nu$	Effective Poisson's ratio
$\mu_{E/E_0}$	Mean of effective normalized Young's modulus
$\sigma_{E/E_0}$	Standard deviation of effective normalized Young's modulus
$\mu$	Mean
$\mu_\nu$	Mean of $\nu$
$\mu_K$	Mean of effective bulk modulus
$\mu_S$	Mean of effective shear modulus
$\rho$	Correlation of coefficient
$\sigma, \sigma^2$	Standard deviation, variance
$\sigma_{(A)}^2$	Variance after local averaging
$\sigma_\nu$	Standard deviation of $\nu$
$\tau$	Difference between points in the field
$\Phi[.]$	Standard normal cumulative distribution function

Table 1. Different input void properties.

Case	$n$	$\Theta$
1	0.2	0.2
2	0.2	0.7
3	0.7	0.2
4	0.7	0.7